Multiscale structure of sheet nacre

Marthe Rousseau[a], Evelyne Lopez[a], Philippe Stempflé[b, c], Marcel Brendlé[b], Loïc Franke[d], Alain Guette[d], Roger Naslain[d] and Xavier Bourrat[e]

[a]Museum National d'Histoire Naturelle, Département des Milieux et Peuplements Aquatiques, UMR 5178 : CNRS-MNHN: «Biologie des Organismes Marins et Ecosystèmes», 7, rue Cuvier 75005 Paris, France
[b]Institut de Chimie des Surfaces et des Interfaces, ICSI, 15, rue Jean Starcky 68057 Mulhouse, France
[c]Ecole Nationale d'Ingénieurs de Tarbes, Laboratoire Génie de Production- Equipe Interfaces et Matériaux Fonctionnels, 47 avenue d'Azereix, 65016 Tarbes, France
[d]Université Bordeaux 1, Laboratoire des Composites Thermo-Structuraux, LCTS, 3 allée de la Boétie, 33600 Pessac, France
[e]Institut des Sciences de la Terre d' Orléans, 1A rue de la Ferollerie, 45071 Orléans cedex 2, France

Abstract

This work was conducted on *Pinctada maxima* nacre (mother of pearl) in order to understand its multiscale ordering and the role of the organic matrix in its structure. Intermittent-contact atomic force microscopy with phase detection imaging reveals a nanostructure within the tablet. A *continuous* organic framework divides each tablet into nanograins. Their shape is supposed to be flat with a mean extension of 45 nm. TEM performed in the darkfield mode evidences that at least part of the intracrystalline matrix is crystallized and responds like a 'single crystal'. The tablet is a 'hybrid composite'. The organic matrix is continuous. The mineral phase is thus finely divided still behaving as a single crystal. It is proposed that each tablet results from the coherent aggregation of nanograins keeping strictly the same crystallographic orientation thanks to a hetero-epitaxy mechanism. Finally, high-resolution TEM performed on bridges from one tablet to the next, in the overlying row, did not permit to evidence a mineral lattice but crystallized organic bridges. The same organic bridges were evidenced by SEM in the interlaminar sequence.

Keywords: Nacre; Aragonite; Nanocomposite; Biomineralization; AFM; TEM

1. Introduction

This paper is focused on the composite structure of nacre for its future use as a natural bioceramic for bone regeneration [1]. The structure of nacre is already well documented by the works of Wada [2], Wise [3], Grégoire [4] and Mutvei [5]. A long tradition of structural analysis exists in this field, often conducted by electron microscopy. Grégoire et al. [6] already used this technique in 1955 to evidence the interlaminar sheet of organic matter. Bevelander and Nakahara [7] later introduced decisive insights to establish the compartment theory. Meanwhile, Erben and Watabe in 1974 discussed some aspects of this theory [8]. Concomitantly, Mutvei [5], [9] and [10] also cleverly played with preparation procedures to highlight certain fine details related to biocrystal growth. Very recently, the sophisticated

method of cryo-TEM was employed to cross-check the fine structure usually observed by dehydration and staining techniques with the same matrix but hydrated and vitrified at low temperature [11]. The composite structure was also studied, particularly the role of the organic matrix by a bio-chemical approach [12], [13], [14], [15], [16], [17], [18], [19] and [20]. It resulted in different models proposed by Schäffer et al. [21] and Levi-Kalisman et al. [11].

In a companion paper [22] we arrived to the conclusion that mineralization of the compartment follows a Voronoi tiling model. Here, we propose to study the structure of the organic matrix using techniques such as darkfield TEM or intermittent-contact atomic force microscopy (AFM) coupled with phase imaging (AFM in taping mode).

2. Materials and methods

2.1. X-ray diffraction

Texture analyses were performed on an X-ray pole figure goniometer with an Euler attachment (Siemens D5000) and a copper anticathode. Pole figures were obtained on three rays of aragonite successively, 002, 012 and 111, in order to take each reciprocal direction into account. Data processing and diagram plotting were performed with the software included in the package. The samples were cut on different places on the inner shell nacre layer of a giant oyster, *Pinctada maxima*, as shown in the diagram in Fig. 1. The samples of 25×25 mm^2 were as flat as possible, one being 3 mm in diameter (sample T). A Schulz setting in reflection was used. $\theta°$ and $2\theta°$ angles were kept constant on the maximum of the reflection for the (hkl) plane distribution to be analyzed. The angle, ϕ, namely the rotation of the sample on itself, was computerized with a step of 5° starting at 0° and increasing up to 360°. The angle χ, or Euler angle, was computerized with a step of 4°, from 0° to 90° and a counting time of 10 s. As the rocking of the χ angle up to χ=90° is too high and the incident beam too parallel to the sample, the Schulz method in reflection does not make it possible to obtain a complete figure in the best conditions: over a value of χ>65° the intensities recorded are attenuated by a defocusing phenomenon (corrections were not made in this work).

2.2. Atomic force microscopy (AFM)

The microscope used was a *Dimension 3000* connected to an electronic controller, the *Nanoscope IIIa*™ produced by *Digital Instruments* (USA). The spatial and vertical resolutions are less than 1 nm and the field is between 100 nm and 100 μm. The images recorded in this work were taken at high resolution (512×512 pixels) by using an intermittent-contact mode (called Tapping Mode™) coupled with phase detection imaging (PDI). The tapping-mode makes it possible to minimize the interactions between the probe and the surface during acquisition and considerably improves the resolution compared to the contact mode [23]. Coupled with PDI, this mode, in addition to the topographic images, provides a map characterizing the variations of the mechanical properties of the scanned surface (phase contrast) [24]. The probe is in SiNi with a round tip of between 5 and 10 nm. The work frequency, the stiffness and the amplitude of cantilever were 270 kHz, 42 N m^{-1} and 25 nm, respectively. The scanning rate was 1.2 μm s^{-1}. Data were collected in air and at room temperature after polishing parallel to the nacre surface.

2.3. Transmission electron microscopy

Two types of samples were selected: (i) nacre cut from the recent shell of *P. maxima*; and (ii) from old and dry nacre from collections. First, a mechanical thinning was obtained on small slides, 3 mm in diameter. At a thickness of about 80 μm, both sides were polished and then glued on to a single-hole copper grid. Ion milling was then performed using a Gatan DuoMill at room temperature. Thinning was continued until electron transparency was obtained. Artifacts due to sampling appeared to be reduced and limited to the edge of the hole. For beam stability reasons, the old nacre was preferred for the preparation of high-resolution images.

Numerous TEM studies have been carried out on nacre over the last 50 years. Both traditional sample preparations of ultramicrotomy or ion-beam milling have been used. Both techniques are known to introduce specific artifacts. Ultramicrotomy generally breaks the samples, producing splinters. Within each splinter the structures remain, enabling full analysis [25]. In this case the interfaces are destroyed. It is hard to work on the interlaminar matrix with this technique. Ion-beam milling carries the danger of carbonization of the organic matrix. Using thermal gravimetric analysis, we have measured that nacre can in fact sustain temperatures as high as 230 °C without any mass change under air. Several groups have used this technique initiated in this field by Towe and Hamilton [26]. Aksay's group, in particular, fully discussed this point, reaching the conclusion that radiolysis is probably very minor [27].

Observations were conducted in a Philips CM30ST at 300 kV with a point resolution of $\delta = 0.2\,\mathrm{nm}$. Darkfield technique was performed using an objective opening of 2.15 nm^{-1}. Once the stage is tilted in order to get parallel to the axes, the beam is tilted near the transmitted spot avoiding any mineral reflection. In these conditions the contrast is provided by the crystallized organic matrix (mineral spots are eliminated by the small objective aperture).

3. Results and discussion

3.1. Long range orientation of aragonite crystals

Pole figures obtained on (0 0 2) planes show a preferential orientation of the aragonite crystals. This is indicated by the single pole which appears at the origin of the angles in Fig. 2 for sample T (3 mm in diameter). This orientation is also homogeneous for samples as large as 25×25 mm^2. That means that all the *c*-axes in the sample are parallel to each other and perpendicular to the surface of the nacre shell. The textural pattern of the (0 1 2) planes exhibits two poles (Fig. 2) as a ‘single crystal-like pattern’. That means that all the crystals are also mutually oriented in nacre with their *b*-axes parallel at long range (25×25 mm^2) and hence also their *a*-axes are parallel. That fact is confirmed by the measurement on the 111 reflection (Fig. 2). Four poles appear, corresponding to the symmetry of the lattice and with the $\underline{\delta}$ angles corresponding to 111 reflections. The same local orientation of the aragonite platelets is observed in the three areas sampled on the nacre shell, numbered 1, 2 or 3. Fig. 1b shows that the respective *a*- and *b*-axes of the different samples rotate according to their location over the shell. Wada [28] had already measured that the *b*-axes get a radial orientation, the direction of shell growth. Many scientists have reported similar results on bivalve nacre orientation [12], [13], [29] and [30]. In our case, this point was verified except for sample 1.

Here the pole figures have to be interpreted as a common orientation of crystals at long range. A very slight dispersion is real and can occur in the same layer laterally or from one layer of tablets to another. Confirmation has been obtained with TEM. Locally, the orientation between two neighbouring tablets (from one row to the other) can be strictly the same, as for a single crystal. At long range, however, the orientation is only 'statistical'. This phenomenon was described by Wada [31] as the 'mosaic single crystal'. It is interesting to note that there is no drastic enlargement of the poles when considering samples of 25×25 mm^2. This observation was already pointed out by Chateigner et al. [32] with the measure of the 'textural strength' in *Pinctada margaritifera*.

3.2. Nanostructure of the platelet by AFM

In *Tapping Mode*^{TM} coupled with PDI, two types of determination are simultaneously obtained: a Height Map (Fig. 3a) enables monitoring of the flatness of the sample (polished parallel to tablets), and the Phase Contrast Map (Fig. 3b) enables the detection of variations in composition, adhesion, friction, viscoelasticity or other properties, including the detection of the different composite components [24]. Technically, the images in Fig. 3 and Fig. 4 are obtained by measuring the phase difference between the excitation signal and the cantilever response. This information can be related to the dissipation of energy during the interaction of the tip on the surface. These data are related to local variations of the material. The resulting phase contrasts are often difficult to interpret because of the complex interactions of chemical and physical effects [33] and [34]. Here, the interactions can be related to the drastic difference of the elastic properties of the intracrystalline organic matrix regarding those of the mineral phase. The NiSi tip of the AFM is chemically non-reactive: chemical interactions with the sample are more than likely negligible with respect to the contrast expected with the elastic modulus variations between mineral and organic phases [35].

It has long been demonstrated that a intracrystalline matrix is present within the tablets [5], [10] and [36] but its relationship with the mineral has never been shown at the nanometre scale.

Figs. 3a and b evidence *mineral nanograins surrounded by an organic phase*, owing to the strong elastic modulus contrast between proteins and aragonite. Fig. 4 is another phase-contrast picture recorded on a wider field of 1×1 μm^2. The organic matrix is organized as in the form of a 'foam' with very thin walls and closed cells. The mineral nanograins are thus encapsulated inside the organic framework (vesicle). Post-processing treatment was applied to the different images (grain analysis using the software *SPIP*™ by *Image Metrology ApS*). This makes it possible to determine the morphology (size and shape) of the nanocrystals. A mean nanograin size of 44 nm (±23) was found. The tablet responds as a single-crystal [37]. It is in fact made up of a coherent aggregation of nanograins.

Finally, Fig. 3 and Fig. 4 clearly show that the organic framework is continuous within the tablet; nothing evidences that the mineral is also continuous.

3.3. Laminate feature of the tablet by TEM brightfield

Brightfield TEM in Fig. 5 shows the tablets and the interlaminar organic matrix (ILOM) as well as the intercrystalline organic matrix (ICOM) between two neighbouring tablets in the same row. Sampling artifacts produced by the ion-milling technique can be easily recognized (noted Amorph.) with the loss of features and full amorphization near the edge of the hole

(noted Ho). It has long been established that tablets diffract as a single crystal and most of the time, sets of tablets in a pile (cross section) also diffract as a single crystal [19]. This was recently approached using a synchrotron microbeam mapping technique for abalone [38]. This is confirmed in the present work for *P. maxima* (electron diffraction patterns are not shown). Transmission of the crystallographic orientation along the pile was attributed to the continuous growth of carbonate, thanks to mineral bridges from one row to the overlying one, in the case of *Haliotis rufescens* [21], *Mytilus edulis* [19] and recently on *Haliotis iris* [39]. In this work, as we saw by AFM, the *mineral continuity is not proved inside the tablet and is difficult to evidence from one row to the other* (see below).

Scanning electron microscopy provided evidences of the laminate structure of the tablet (Fig. 6) indicating that the nanograins are very likely nanotablets (AFM was not processed in cross section). This last micrograph was obtained in the conditions described in a previous work [2].

3.4. Continuity of the organic framework in the tablet (TEM)

Chitin or proteins have ordered structures which diffract [40] and [41]. Their diffusion coefficient and preferred orientation are supposed to be weaker, compared to those of the mineral lattice. The contrast related to the organic and mineral phases is anyway difficult to distinguish in most cases. By using filtering in the reciprocal space, known as darkfield TEM, it is possible to select one of the spatial frequencies ($s=\lambda/\theta$) related to the organic matrix by means of a small objective aperture and obtain it in contrast, despite the presence of the mineral phase which remains extinguished. That is the way the organic framework can be studied, in situ.

Fig. 7 is a darkfield image obtained by filtering the reciprocal space with a very small objective aperture, avoiding the aragonite spots. Thus, *only the organic matrix is in contrast* (*part of it only*). First, the highest contrast comes from the organic matrix of the interlaminar region.

Second and most importantly, this technique evidences the presence of the intracrystalline organic matrix in a different way as compared to AFM. In each tablet, the intracrystalline matrix is seen to diffract under the form of tiny spots: all the spots get in contrast together in the tablet. The variation of the contrast from one tablet to the other in Fig. 7 suggests that *the intracrystalline organic matrix reacts as a* '*single crystal*' *network* (or at least a part of it). If the organic matrix is oriented under the Bragg angle it brightens all over the tablet (case of tablet A). If it is just slightly misoriented, only a faint contrast appears (tablet B). This is related to a Bragg tolerance phenomenon classically observed in the case of small coherent domains such as these. In other tablets (as C) the intracrystalline organic network is extinguished because not selected in this direction or not under the Bragg angle. It is relevant to note that distortions appear in tablet A. Are they related to sampling artefacts or are they real? More work is needed on this question.

Finally, the relationships between the intracrystalline and interlaminar matrix are noteworthy. The interlaminar matrix brightens substantially when the intracrystalline matrix also brightens. If the neighbour is also in contrast, both sides of the interlaminar sandwich are bright (single arrow), but only one side is bright if the neighbour is extinguished (double arrow). When the two neighbours are extinguished, the interlaminar matrix is also

extinguished or only faintly in contrast (triple arrow). The median layer of the interlaminar sequence is formed by a porous layer appearing as a succession of bridges in cross section (studied by TEM high resolution in the next section) and imaged flat-on by SEM (Fig. 8) in a previous work [22].

3.5. High-resolution TEM on the interlaminar matrix

Electron diffraction has not the required spatial resolution to process a diffraction pattern on a single bridge. Instead, high-resolution TEM was performed on bridges, as shown in Fig. 9 (corresponding in location and scale to the square drawn in Fig. 7). Then, Fast Fourier Transforms (FFT) was used to analyze the different lattice types: either orthorhombic for the aragonite or others, attributed to the organic matrix. In the case of Fig. 7 FFT produced in the insets shows that there is no orthorhombic pattern: the FFT distances for the organic bridge and the lateral interlaminar organic layer are the same (but not the same orientations, here spacings of 0.19, 0.16 and 0.12 nm). The FFT analysis of HR-TEM images was performed on many different areas by tilting the plate of the microscope. Aragonite spots were never observed in the bridges patterns, in contrast to those recorded in the tablets (see the orthorhombic symmetry of the FFT of Fig. 10). In *Pinctada* nacre, the bridges are very likely the cross section of the alveoli organic layer shown in Fig. 8 observed in a previous work [22]. Fig. 9 was obtained for one of the many possible orientations of the interlaminar matrix. It confirms that this organic matrix is highly crystallized. Many moiré fringes appear due to multidiffraction within the organic matrix. No exhaustive Fourier analysis was performed at that time on the different lattice distances observed in the organic matrix.

4. Concluding remarks

1. The tablet of nacre, the biocrystal, does diffract as a single crystal but is made up of a continuous organic matrix (intracrystalline organic matrix), which breaks the mineral up into coherent nanograins (~45 nm mean size, flat-on) which share the same crystallographic orientation.

2. The single crystal-like mineral orientation of the tablet is supposedly created by the heteroepitaxy of the intracrystalline organic matrix. This is a strong hypothesis because this work demonstrates at the same time that this intracrystalline matrix is well crystallized (i.e. periodic) and diffracts as a ‘single crystal’ too (darkfield TEM mode, Fig. 7).

3. Neighbouring tablets above and below can maintain a common orientation, which again raises the issue of the transmission of mineral orientation from one row to the next. Bridges are well identified in *Pinctada* between successive rows in the pile, but all of those analyzed were organic and not mineral.

4. Finally, this work provides an interesting hypothesis to explain why the tablets first grow with a cylindrical shape and then turn polygonal when contacting each other [22]. The existence of nanograins encapsulated in an organic vesicle raises the hypothesis of an aggregation-like control of the extension of the tablet by the organic template and not directly at the atomic level.

Acknowledgements

Professor David Smith is thanked for the English presentation and for suggesting some descriptive improvements.

References

[1] E. Lopez, S. Berland, C. Camprasse, G. Camprasse and C. Silve, Demonstration of the capacity of nacre to induce bone formation by human osteoblasts maintained in vitro, *Tissue Cell* **24** (1992), pp. 667–679.

[2] K. Wada, Crystal growth of molluscan shells, *Bull Natl Pearl Res Lab* **7** (1961), pp. 703–828.

[3] S.W. Wise, Microarchitecture and mode of formation of nacre (mother of pearl) in Pelecypods, Gastropods and Cephalopods, *Eclogae geol Helv* **63** (1970), pp. 775–797.

[4] Grégoire C. Structure of the molluscan shell. In: Florfin M, Scheer BT, editors. Chemical zoology. vol. II. New York, 1972. p. 45–102.

[5] H. Mutvei, On the internal structures of the nacreous tablets in molluscan shells, *Scan Electr Micros* **II** (1979), pp. 457–462.

[6] C. Grégoire, G. Duchateau and M. Florkin, La trame protidique des nacres et perles, *Ann Océano* **Tome XXXI** (1955), pp. 1–36.

[7] G. Bevelander and H. Nakahara, An electron microscope study of the formation of nacreous layer in the shell of certain bivalve molluscs, *Calc Tiss Res* **3** (1969), pp. 84–92.

[8] H.K. Erben and N. Watabe, Crystal formation and growth in bivalve nacre, *Nature* **248** (1974), pp. 128–130.

[9] H. Mutvei, On the micro and ultrastructure of conchiolin in the nacreous layer of some recent and fossil molluscs, *Stockhlom Centr Geol* **20** (1969), pp. 1–17.

[10] H. Mutvei, Ultrastructure of the mineral and organic components of molluscan nacreous layers, *Biomineralization Res Rep* **2** (1970), pp. 48–72.

[11] Y. Levi-Kalisman, G. Falini, L. Addadi and S. Weiner, Structure of the nacreous organic matrix of a bivalve mollusk shell examined in the hydrated state using Cryo-TEM, *J Struct Biol* **135** (2001), pp. 8–17.

[12] S. Weiner and W. Traub, X-ray diffraction study of the insoluble organic matrix of mollusc shells, *Eur Biochem Soc* **111** (1980), pp. 311–316.

[13] S. Weiner and W. Traub, Macromolecules in mollusc shells and their functions in biomineralization, *Philos Trans R Soc Lond B* **304** (1984), pp. 425–434.

[14] S. Weiner and L. Addadi, Acidic molecules of mineralized tissues: the controllers of crystal formation, *Trends Biochem Sci* **16** (1991), pp. 252–256.

[15] S. Mann In: S. Mann and R.J.P. Williams, Editors, *Biomineralization: chemical and biological perspectives*, VCH Verlags Gesellschaft, Weinheim (Germany) (1989), pp. 146–148.

[16] S. Mann, D.D. Archibald, J.M. Didymus, T. Douglas, B.R. Heywood, T.C. Meldum and N.J. Reeves, Crystallization at inorganic-organic interfaces: biominerals and biominetics synthesis, *Science* (1993), p. 261.

[17] G. Falini, S. Albeck, S. Weiner and L. Addadi, Control of aragonite or calcite polymorphism by mollusk shell macromolecules, *Science* **271** (1996), pp. 67–69.

[18] A.M. Belcher, X.H. Wu, R.J. Christensen, P.K. Hansma, G.D. Stucky and D.E. Morse, Control of crystal phase switching and orientation by soluble mollusc-shell proteins, *Nature* **381** (1996), pp. 56–58.

[19] Q.L. Feng, H.B. Li, F.Z. Cui and H.D. Li, Crystal orientation domains found in the single lamina in nacre of the *Mytilus edulis* shell, *J Mater Sci Lett* **18** (1999), pp. 1547–1549.

[20] J.B. Thompson, J.T. Poloczi, J.H. Kindt, M. Michenfelder, B.L. Smith, G. Stucky, D.E. Morse and P.K. Hansma, Direct observation of the transition from calcite to aragonite growth as induced by abalone shell proteins, *Biophys J* **79** (2000) (6), pp. 3307–3312.

[21] T.E. Schäffer, C. Ionescu-Zanetti, R. Proksch, M. Fritz, D.A. Walters, N. Almqvist, C.M. Zaremba, A.M. Belcher, B.L. Smith, G.D. Stucky, D.E. Morse and P.K. Hansma, Does abalone nacre form by heteroepitaxial nucleation or by growth through mineral bridges?, *Chem Mater* **9** (1997), pp. 1731–1740.

[22] M. Rousseau, E. Lopez, A. Couté, G. Mascarel, D.C. Smith, R. Naslain and X. Bourrat, Sheet nacre growth mechanism: a Voronoi model, *J Struct Biol* **149** (2005), pp. 149–157.

[23] J.P. Aimé, L. Boigard, G. Nony and G. Couturier, Influence of nanocontact dissipation in Tapping-mode: attempt to extract quantitative information on the surface properties with the local force probe method, *J Chem Phys* **114** (2001), pp. 4945–4954.

[24] S.N. Magonov, V. Elings and M.-H. Whangbo, Phase imaging and stiffness in tapping-mode atomic force microscopy, *Surf Sci* **375** (1997), pp. 385–391.

[25] K. Gunnison, M. Sarikaya, J. Liu and I.A. Aksay, Structure-mechanical property relationships in a biological ceramic-polymer composite: nacre. In: I.A. Aksay, E. Baer, M. Sarikaya and D.A. Tirrel, Editors, *Hierarchically structured materials, Proc MRS 255*, MRS, Pittsburg USA (1992), pp. 171–183.

[26] K.M. Towe and G.H. Hamilton, Ultrastructure and inferred calcification of the mature and developing nacre in bivalve mollusks, *Calcif Tissue Res* **1** (1968), pp. 306–318.

[27] M. Sarikaya, J. Liu and I.A. Aksay, Nacre: properties, crystallography, morphology and formation. In: M. Sarikaya and I.A. Aksay, Editors, *Biomimetics: design and processing of materials*, AIP Press, USA (1995), p. 35.

[28] K. Wada, The crystalline structure on the nacre of the pearl oyster shell, *Japan Soc Scient Fish* **24** (1958) (6 and 7), p. 422.

[29] S. Weiner and L. Addadi, Design strategies in mineralized biological materials, *J Mater Chem* **7** (1997) (5), pp. 689–702.

[30] A.G. Checa and A. Rodriguez-Navarro, Self-organisation of nacre in the shells of Pterioida (Bivalvia: Mollusca), *Biomaterials* **26** (2005), pp. 1071–1079.

[31] K. Wada, Nucleation and growth of aragonite crystals in the nacre of some bivalve molluscs, *Biomineralization* **6** (1972), pp. 141–159.

[32] D. Chateigner, C. Hedegaard and H.-R. Wenk, Mollusc shell microstructures and crystallographic textures, *J Struct Geol* **22** (2000), pp. 1723–1735

[33] J.P. Cleveland, A.E. Schmid and V.B. Elings, Energy dissipation in tapping-mode atomic force microscopy, *Appl Phys Lett* **72** (1998), pp. 2613–2615.

[34] J. Tamayo and R. Garcia, Relationship between phase shift and energy dissipation in Tapping-mode scanning force microscopy, *Appl Phys Lett* **73** (1998), pp. 2926–2928.

[35] V. Lafon, E. Paris and A. Henriet, The use of AFM to atmospheric particles, case of car exhaust particles, *Digital Instrum Appl Note* (2000), pp. 2–3.

[36] N.J. Schmidt, Die Bausteine des Tierkörpers in Polarisierten Lichte, Cohen, Bonn (1924).

[37] J. Liu, M. Sarikaya and I.A. Aksay, A hierarchically structured model composite: a TEM study of the hard tissue of red abalone, *Mater Res Soc Symp Proc* **255** (1992), pp. 9–17.

[38] E. Di Masi and M. Sarikaya, Synchrotron X-ray microbeam diffraction from abalone shell, *J Mater Res* **19** (2004) (5), pp. 1471–1476

[39] F. Song, X.H. Zhang and Y.L. Bai, Microstructure and characteristics in the organic matrix layers of nacre, *J Mater Res* **17** (2002), pp. 1567–1570

[40] H. Nakahara, G. Bevelander and M. Kakei, Electron microscopic and amino acid studies on the outer and inner shell layers of *Haliotis rufescens*, *Venus, Japan J Malacol* **41** (1982), pp. 33–46.

[41] S. Weiner, Y. Talmon and W. Traub, Electron diffraction of mollusc shell organic matrices and their relationship to the mineral phase, *Int J Biol Macromol* **5** (1983), pp. 325–328.

Figures

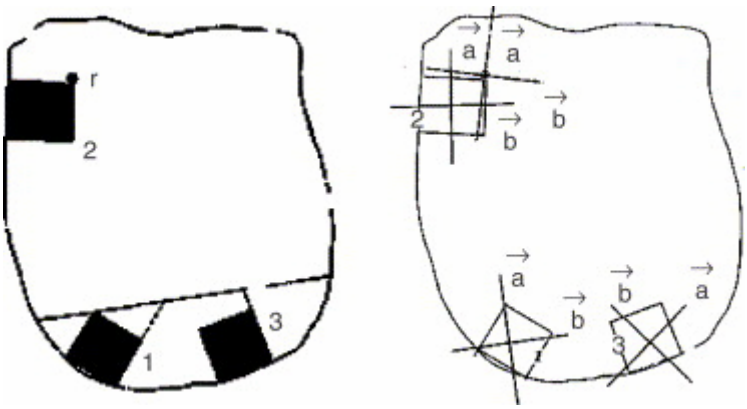

Fig. 1. Sampling for pole figures analysis on the internal sheet nacre of *P. maxima* (a) and orientation of the *a*-and *b*-axes of aragonite for the different samples (square with 25 mm sides, T sample is 3 mm in diameter) (b).

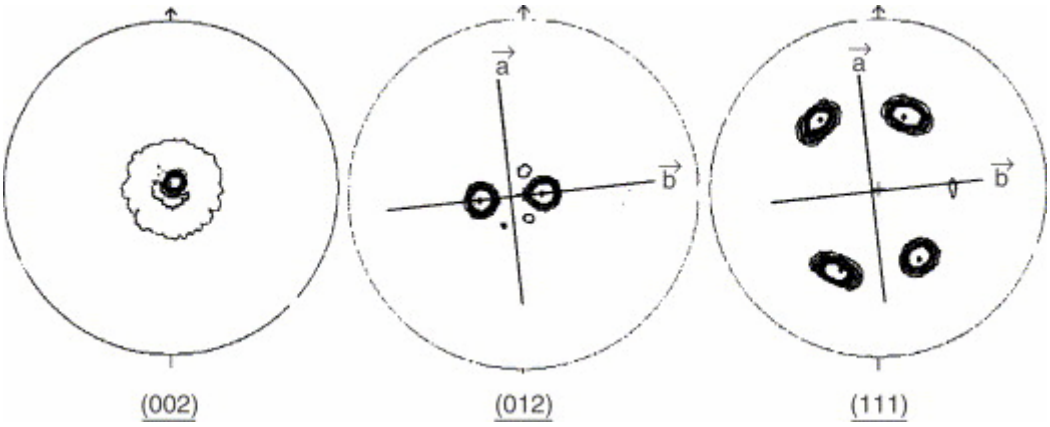

Fig. 2. Pole figures obtained on the nacre layer of *P. maxima* (sample T). All the aragonite tablets maintain the same orientation at long range.

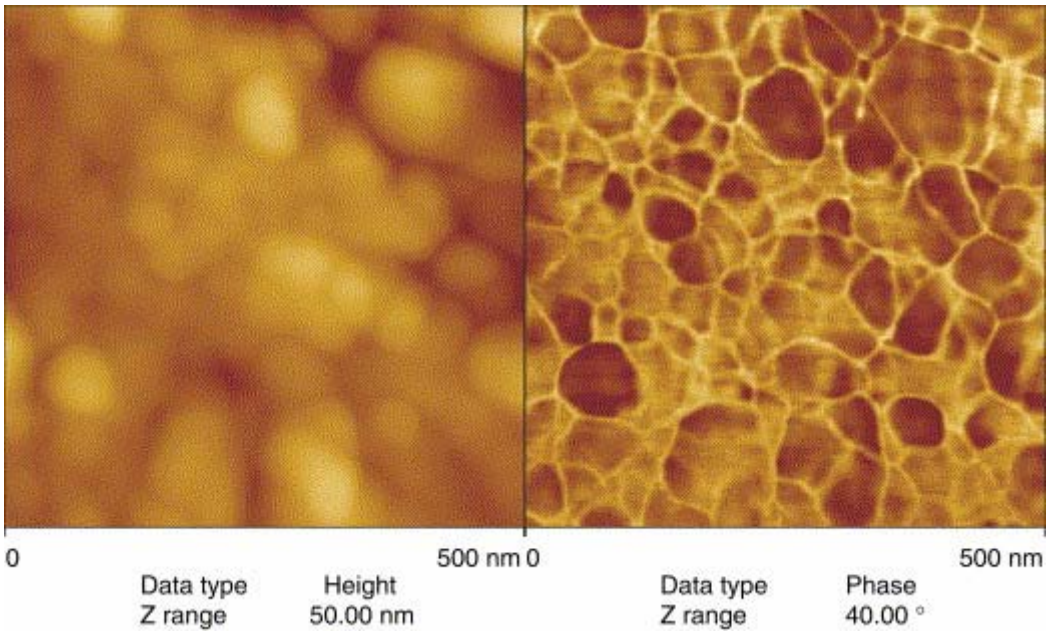

Fig. 3. AFM images of the same polished surface of nacre tablets in tapping-mode (polished with tablets flat-on): (a) Topography of the surface (Height); (b) Picture in phase contrast showing the foam-like structure of the intracrystalline organic matrix.

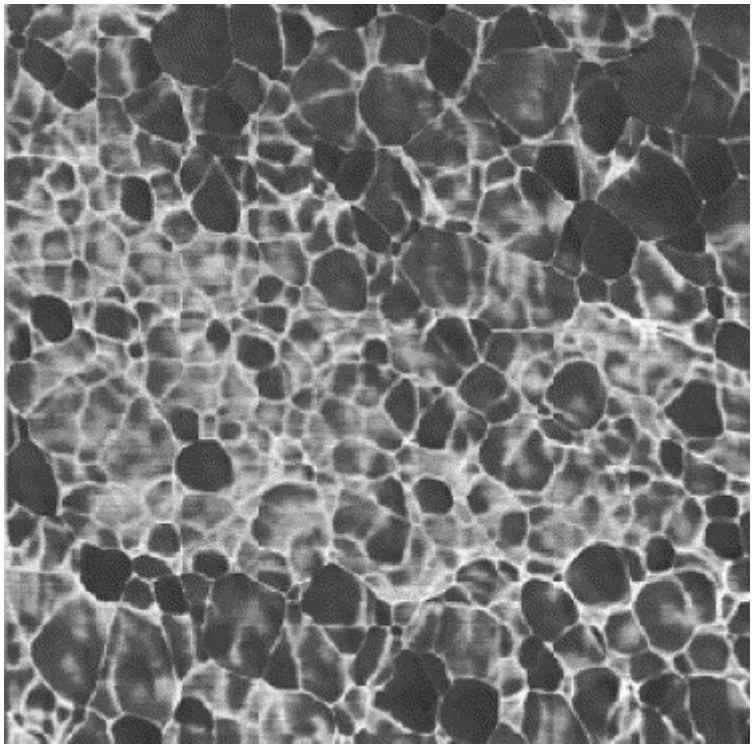

Fig. 4. AFM picture in phase contrast (same as Fig. 3b) with a wider field (1×1 μm^2).

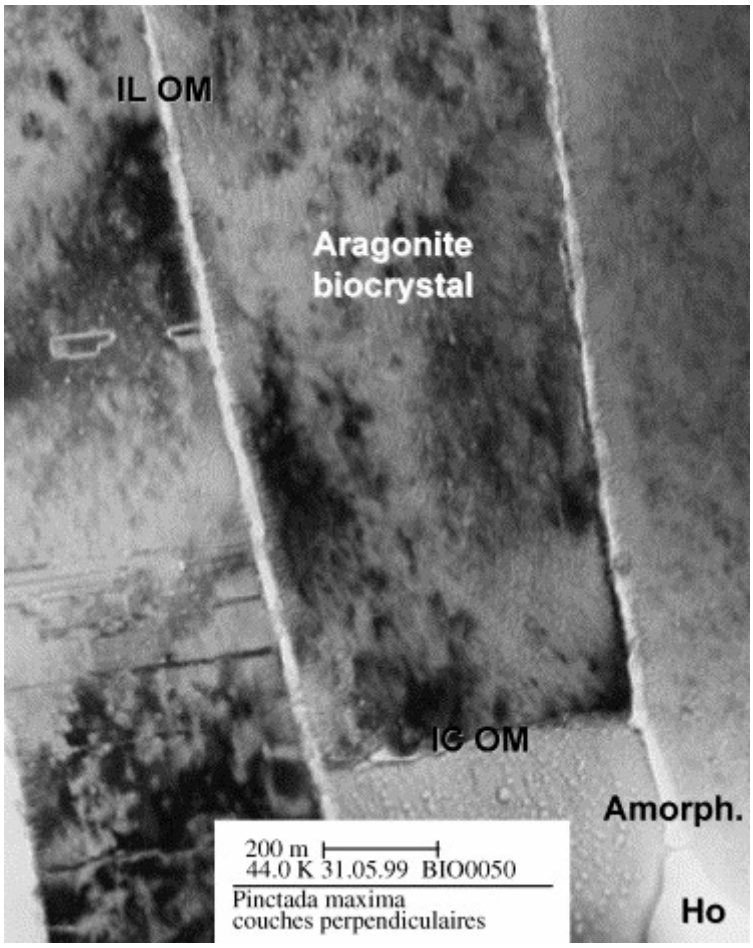

Fig. 5. Contrasted brightfield TEM image showing the aragonite biocrystals (Ho: hole, Amorph.: amorphized area, ICOM: intercrystalline organic matrix, ILOM: interlaminar organic matrix).

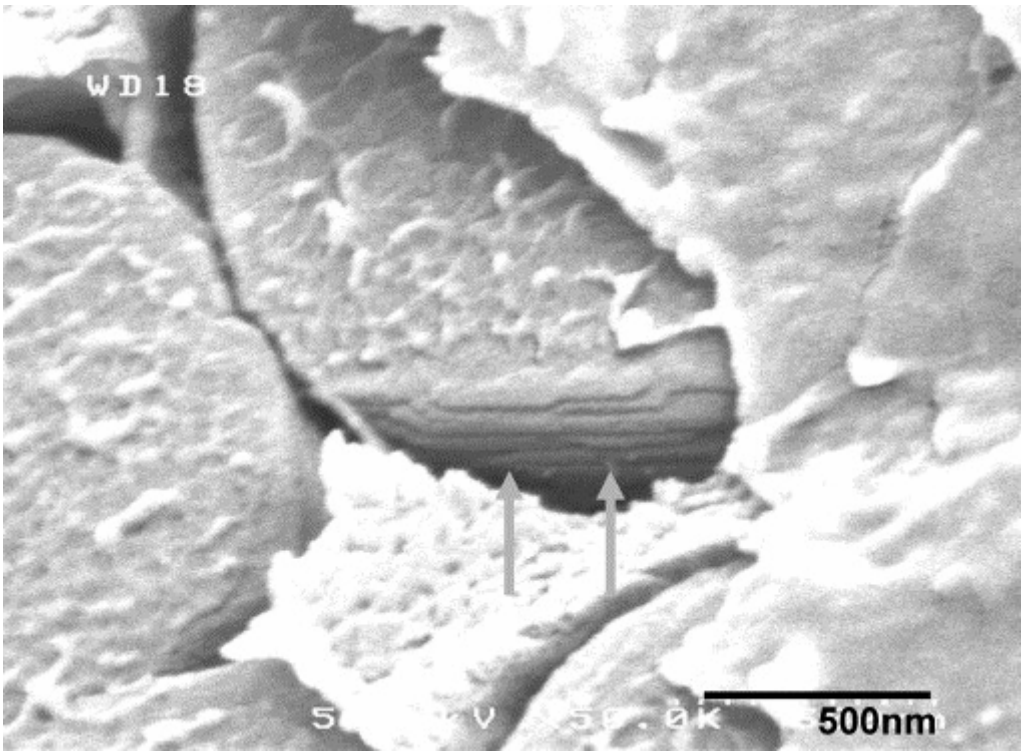

Fig. 6. Growing tablets showing the laminate structure (SEM observation in conditions described in Ref. [22]).

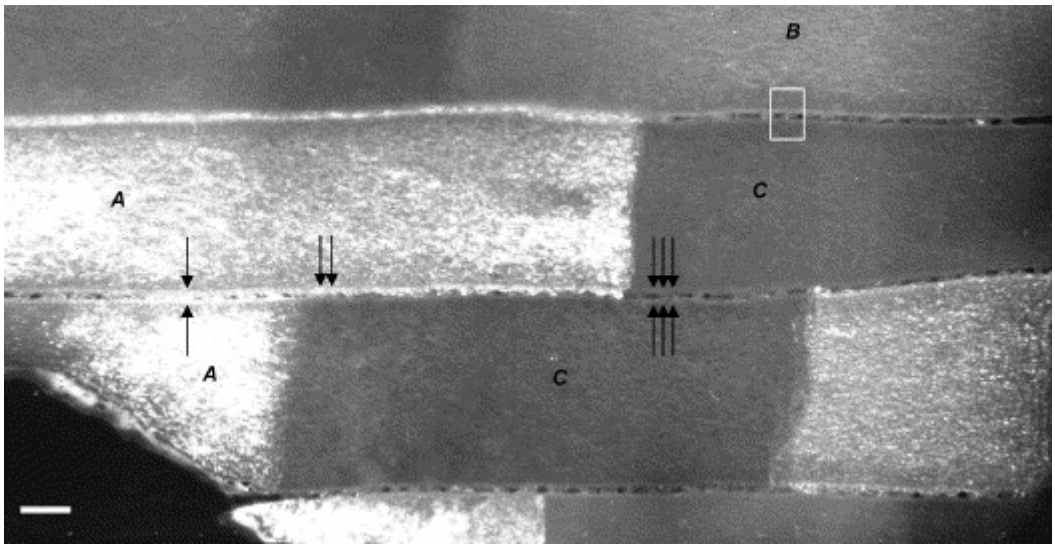

Fig. 7. Darkfield TEM image of nacre evidencing the crystalline structure of the organic matrix (bar is 100 nm). Organic matter is in contrast when under Bragg conditions whilst the mineral phase remains systematically extinguished. The square is the zone that is observed in HR-TEM in Fig. 9.

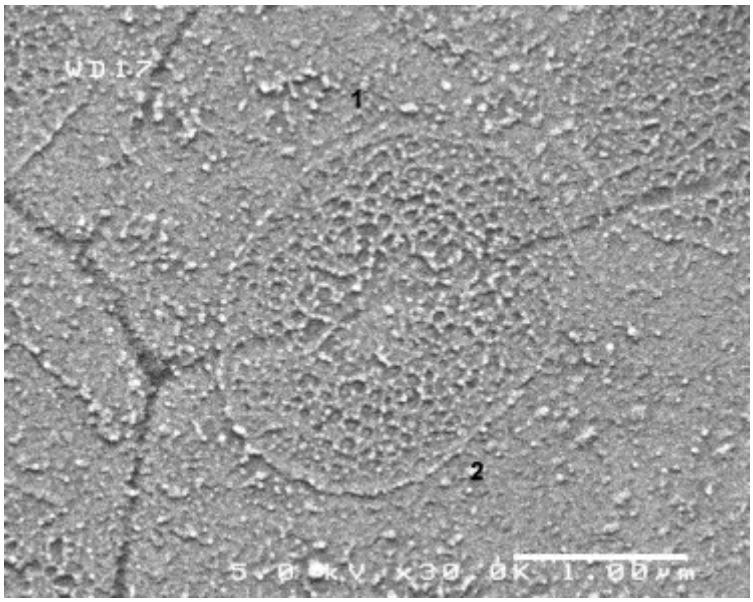

Fig. 8. Fracture surface in the incipient nacre zone showing the alveoli organic structure developing under the tablets (removed with the other side during the fracture, see Ref. [22]).

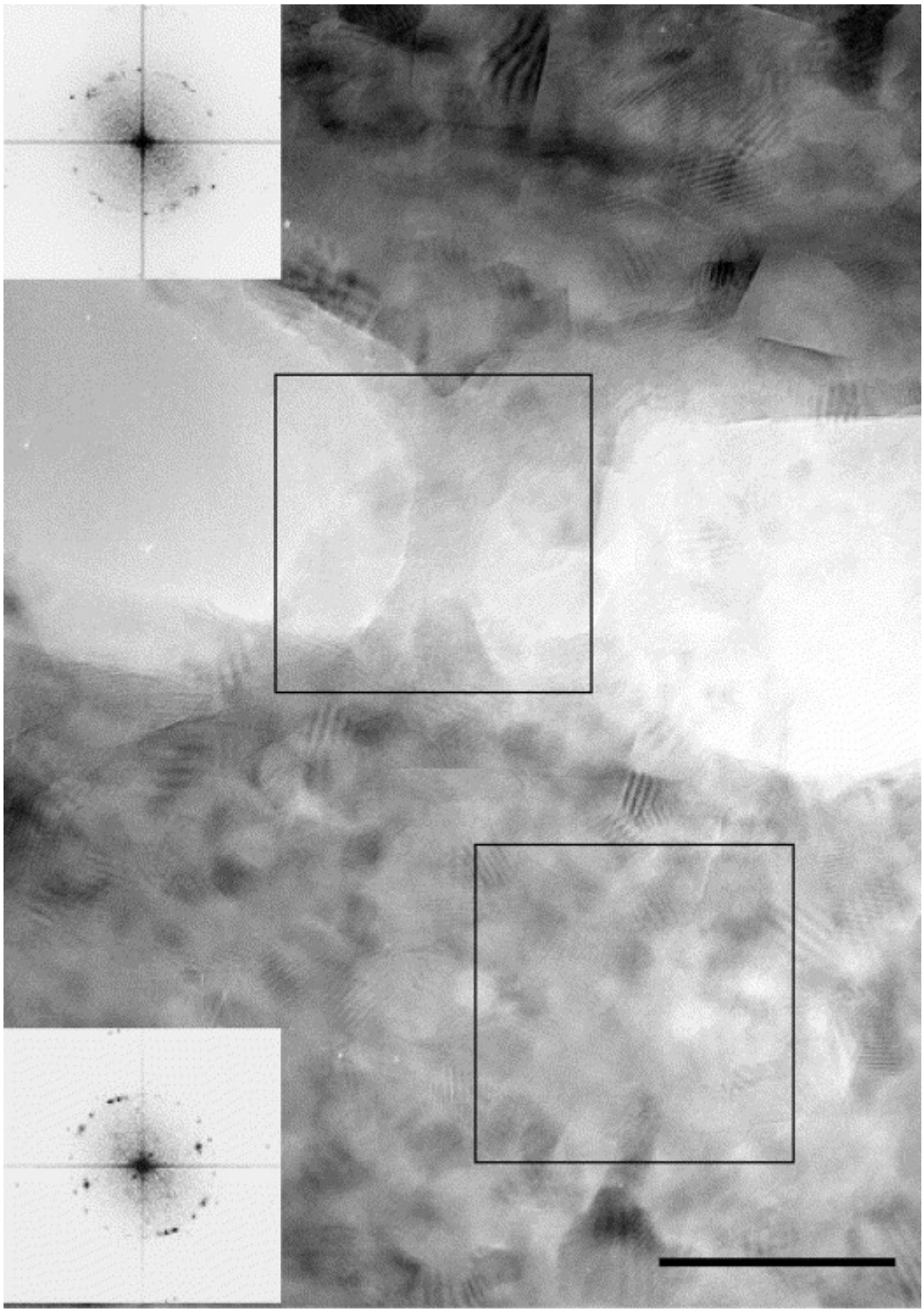

Fig. 9. High-resolution TEM image of a ‘bridge’ in the interlaminar matrix between two tablets. The insets show the Fourier analyses of the two squared regions evidencing only the highly crystallized organic matrix, no $CaCO_3$ orthorhombic lattice (bar is 10 nm).

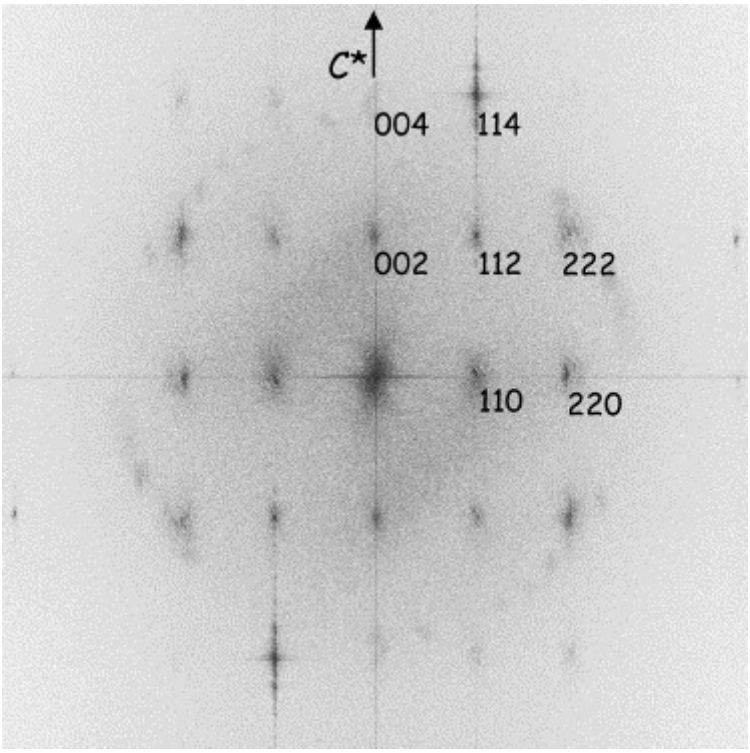

Fig. 10. Fourier pattern obtained from a high-resolution micrograph inside the tablet. Note the superposition of the mineral pattern and spots of the organic matrix.